2 Collisions and cross sections

Elastic collisions are of paramount importance for OHMic heating and energy dissipation into the plasma; inelastic collisions are responsible for all the electronic excitation processes. For both processes, the deductive approach is chosen. By electronic and ionic impact, electrons can be released from surfaces; this process is required for the carrier avalanche in DC discharges, but has regained interest for stabilizing processes in production reactors whose inner surface is subject to various (mostly unintended) coating reactions.

2.1 Introduction

Plasmas are chaotic gaseous systems which contain electrically charged carriers and which maintain themselves by collisions of electric carriers with neutrals. These impacts lead to further carriers, but other energy-consuming processes, such as optical transitions, can be triggered as well. These collisions are subsumed as *inelastic.* Nearly all of the gaseous ionizations are due to collisions between slow heavy particles and rapidly moving electrons. If an electron falls short of the required kinetic energy to excite a heavy particle (atom or molecule), it can but exchange momentum with its counterpart, and we denote this process an *elastic* collision.

This process dominates all other possible collisions since only a very small fraction of electrons have kinetic energies which exceed the threshold of excitation. However, due to the unfavorable mass ratio of individual neutrals/ions over electrons, only a very small portion of energy is exchanged. The lack of efficiency causes an athermal plasma (Chap. 3): Electrons and heavy particles (sometimes even ions alone and neutrals alone) are in separate thermal equilibrium, and the temperatures differ tremendously.

In the case of electron trapping by a neutral molecule or ion, respectively, the electron density is reduced. This process is denoted electron attachment; it will become effective beyond pressures of about some Torr. Below this limit, diffusion processes dominate the loss of electrons: The particles exhibit random walks, caused by stochastic collisions. When the reactor wall becomes a partner of a collision process, the charge is terminated.

With elastic collisions, only a very small fraction of kinetic energy is exchanged between particles which significantly differ in mass, which leads to only a small increase of kinetic energy of the translational energy of the gas constituents, i. e. a small rise in gas temperature. The electron kinetic energy is significantly reduced by inelastic collisions, which cause excitations of molecular rotations, vibrations and eventually electronic transitions. It is this excitation which generates ions, radicals and other dissociation products; furthermore, metastable species can be formed. When these inelastic collisions are possible, they dominate all other processes because of their large losses of energy. All these species can again react among themselves, but they can also relax. An electronic transition is often combined with radiation of light (UV/VIS range), which is specific to the ambient conditions (cf. Chap. 9).

Our interest in these processes is twofold: Elastic scattering is mainly responsible for energy transfer and dissipation of energy; by inelastic scattering, optical levels can be occupied or neutrals are excited to ions, and electrons are generated. For electron generation, we distinguish between certain classes which are denoted primary processes, i. e. thermal emission and field emission, and secondary processes:

- Generation of secondary electrons at the cathode and the walls by particles abundant in energy (γ-reaction): photons, electrons incident to the anode, ions incident to the cathode.

- Ionization by impact by particles abundant in energy in the negative glow and the dark spaces of either electrode (impact by electrons: α-reaction, impact by ions: β-reaction).

Primary processes can be neglected in glow discharges. Ions are produced only by gaseous reactions; otherwise, they can be generated by thermal emission, however, with very low yield [13].

2.2 Elastic collisions

2.2.1 Cross section

In an approximation to first order, the cross section for elastic scattering is adapted from kinetic gas theory, which regards molecules as hard spheres, and its fourfold area is defined as the cross section; we begin with the relation between mean free path λ and particle density n

$$\lambda \approx \frac{1}{n\sigma}. \tag{2.1}$$

The channel of a molecule with cross section σ as inner diameter is now exposed to an electron beam with flux I_0, which is shot into an ensemble of

non-interaction particles. After having covered a certain distance x, the flux has been attenuated to

$$I = I_0 e^{-\mu x} \qquad (2.2)$$

according to BEER and LAMBERT with μ a reciprocal length which can be interpreted as mean free path λ following Eq. (2.1)

$$\frac{1}{\lambda} = n\sigma \qquad (2.3)$$

with n the density of the molecules and σ the cross section of the specific interaction. For a fundamental understanding of the cross section, the integral attenuation of an electron beam, its angular and eventually its energetic dependence are required.

2.2.1.1 Cross section and mean free path in kinetic gas theory. The time τ between two collisions is of the order of $\tau \approx \lambda / <v>$ with $<v>$ the mean thermal velocity. The mean free path λ itself depends on particle density n and cross section σ according to Eq. (2.3) because it roughly scales with the target area of the molecule. In the simple approach of kinetic gas theory, this cross section is the only one considered and is the cross section for elastic scattering (see [14]). In this approximation, the cross section for elastic scattering is independent of temperature (energy) and is tabulated in units of πa_0^2—the cross section of the hydrogen atom with a_0 BOHR's radius (0.529 Å), 8.82×10^{-17} cm^{-2} [sometimes the averaged collision number P_c across 1 cm for a gas at 1 Torr (133 Pa) and 0 °C is found; the relation is $\sigma = 0.283 P_c$ in Å^2]. A typical value for λ is 4.5 cm for nitrogen at 1 mTorr (0.2 Pa).

In fact, the cross section weakly depends on temperature (kinetic energy): With decreasing temperature (reduced molecular speed), it rises slowly due to prolongation of the interaction. For example, by reducing the temperature by 200 °C from +100 °C to −100 °, σ_{el} rises by 30 % for nitrogen and oxygen.

2.2.1.2 Cross section and mean free path in plasmas. This temperature dependence is caused by weak intermolecular forces (polarization), which exhibit a weak r^{-6} dependence for the attractive part of the LENNARD-JONES potential Φ_{LJ}. In plasmas, however, we have bare charges which lead to intense, far-reaching interactions which can be described analytically only in some simple cases. To begin with, we introduce some experimental details for atoms and electrons:

- Atoms
  - In a sputter system operated with argon at 50 mTorr (7 Pa), the mean free path of the argon atoms is approximately 1.54 mm (25 meV Ar, $\sigma_{\mathrm{tot}} = 26$ Å^2).

- Ions
    - The mean free path of ions is considerably smaller. λ for Ar$^+$ ions of medium velocity in argon at 30 mTorr (4 Pa) and 4 eV is about 0.87 mm and rises for 10 eV ions to 1 mm and for 100 eV atoms to 1.4 mm.
    - In ion beam sources which are driven at significantly lower pressures, they are larger by orders of magnitude: For 400 eV Ar$^+$ ions and a gas pressure of 10^{-4} Torr (13 mPa), λ equals 51.6 cm.

- Electrons
    - λ_e of fast electrons in argon [16 eV, which is at the maximum of σ (26 Å^2)] amounts to about 2.5 mm at a pressure of 50 mTorr (7 Pa), corresponding to about 7.5 mm at 20 mTorr (3 Pa).
    - Slower electrons ($E_{kin} \approx 4$ eV) with a smaller σ (9.7 Å^2) show a longer λ_e (at 20 mTorr about 13 mm) which applies also to rapid electrons (λ_e for 100 eV electrons is about 75 mm at 20 mTorr in argon). The frequencies for elastic collisions between electrons and neutrals yield, according to $\nu_m = n\sigma v$:
        * for 1 Torr (133 Pa, 3.54×10^{16} cm^{-3}) 3.8×10^9 s^{-1},
        * for 100 mTorr (13.3 Pa) 382×10^6 s^{-1} and
        * for 10 mTorr (1.3 Pa) 38×10^6 s^{-1}.

2.2.2 Definitions

First, we consider a beam of monoenergetic particles orientated in a parallel direction with respect to the x-axis and exhibiting a flux of N particles per cm^{2}sec (Fig. 2.1).
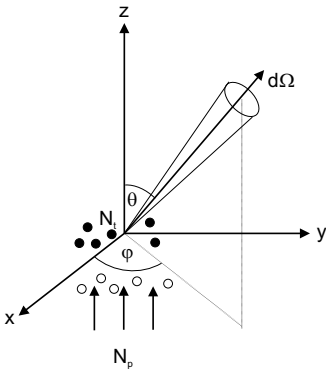

Fig. 2.1. Definition of the differential cross section. N_p projectiles collide with N_t targets and are deflected into dΩ, the differential solid angle element.

In the case of hitting an annular target with area $2\pi b\,\mathrm{d}b$ (b: inner diameter, $b + \mathrm{d}b$: outer diameter), we define the *differential scattering cross section* for solid angle $\mathrm{d}\Omega = 2\pi \sin\vartheta\,\mathrm{d}\vartheta$:

$$\frac{\mathrm{d}\sigma(v,\vartheta)}{\mathrm{d}\Omega} = \frac{b}{\sin\vartheta}\frac{\mathrm{d}b}{\mathrm{d}\vartheta}, \tag{2.4}$$

and the total cross section ("c" for collision)

$$\sigma_{\mathrm{c}}(v) = 2\pi \int_0^\pi \frac{\mathrm{d}\sigma(\vartheta)}{\mathrm{d}\Omega}\,\mathrm{d}\Omega, \tag{2.5}$$

which, in turn, does not allow any statement of the angular dependence. Furthermore, we define the frequency of collision according to

$$\nu_{\mathrm{c}}(v) = n\sigma_{\mathrm{c}}(v)v, \tag{2.6}$$

the mean free path again, but decorated with a subscript "c"

$$\lambda \approx \frac{1}{n\sigma_{\mathrm{c}}(v)} \tag{2.7}$$

and the probability of scattering

$$P_{\mathrm{m}} = \frac{1}{p\lambda}. \tag{2.8}$$

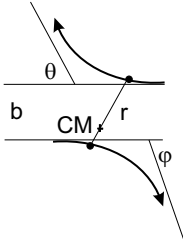The change of momentum is in the center-of-mass system (Fig. 2.2):

Fig. 2.2. Collision between two spheres in the center-of-mass system. b: scattering parameter, θ, φ: scattering angle, CM: center of mass.

$$\Delta \boldsymbol{p} = m\boldsymbol{v}(1 - \cos\vartheta): \tag{2.9}$$

Collisions in the forward direction are minimally weighted ($\cos 0° = 1$), those in the backward direction ($\cos 180° = -1$), however, are considered most prominent: The diffusion is slowed down most effectively by collisions which are orientated backwards.

For the treatment of the transfer of energy and momentum, the most important property is the cross section for momentum transfer, which is $\sigma_{\mathrm{c}}(v)$, but weighted by the factor $1 - \cos\vartheta$:

$$\sigma_{\mathrm{m}}(v, \vartheta) = 2\pi \int_0^\pi \frac{\mathrm{d}\sigma(\vartheta)}{\mathrm{d}\Omega}(1 - \cos\vartheta)\mathrm{d}\Omega, \tag{2.10}$$

along with the *frequency of momentum transfer*:

$$\nu_{\mathrm{m}} = \frac{v}{\lambda} = \nu_{\mathrm{c}}\overline{1 - \cos\vartheta}. \tag{2.11}$$

The cross section of momentum transfer σ_{m} can be extracted from the total collision cross section when its angular dependence is known. For a head-on collision ($\vartheta = 180° = \pi$), we calculate, using the laws of conservation for energy and momentum, the maximum amount of transferred energy to (m the mass of the pushing sphere, M the mass of the stroken sphere)

$$E_{\mathrm{M,kin}} = \frac{4mM}{(m+M)^2}E_{\mathrm{m,kin}} \tag{2.12}$$

which is often rewritten using LANGEVIN's energy loss parameter

$$L = \frac{2m}{m+M} \tag{2.13}$$

eventually yielding [15]

$$E_{\mathrm{M,kin}} = L\frac{2M}{m+M}E_{\mathrm{m,kin}}. \tag{2.14}$$

It can easily be shown that the maximum of this function is given for $m = M$: Collisions between ions with high kinetic energy and slowly moving parent atoms are very effective (cf. Sect. 2.5.2). On the other hand, the energy transfer between an electron and a heavy neutral is negligible ($m_{\mathrm{e}}/m_{\mathrm{Ar}} \approx 70\,000$).

2.3 Elastic collisions between electrons and neutrals

2.3.1 The total cross section

Measurement of the total cross section (sum of all possible scattering processes) was first performed by RAMSAUER using the instrument which is sketched in Fig. 2.3. By exposing a plate of zinc sulfide to UV light, electrons are released at point A by the photoelectric effect. Without collisions, they are forced into orbital motions when a perpendicular magnetic field is applied. They pass all the slots from S_1 to S_5 until they hit the collector C. With elastic collisions, however, electrons are deflected and cannot pass; with inelastic collisions (without deflection), kinetic energy is lost, the orbital diameter increases and these electrons fail to reach the collector as well.

Under a certain pressure p, the electron current is measured in B (current i) and C (current I). For known distance s between S_4 and S_5, the cross section of absorption can be evaluated from the currents i and I at two different pressures p_1 and p_2 according to BEER's law with $\alpha = n\sigma$:
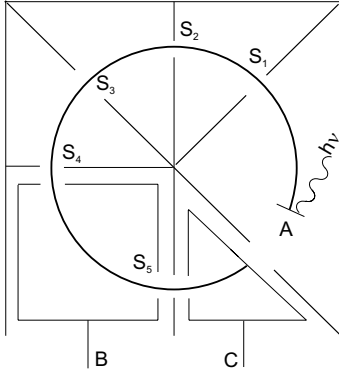
Fig. 2.3. RAMSAUER's apparatus to measure the total cross section [16]. First, electrons are released from a slab made of ZnS. By applying a magnetic field orientated normally to the plane of the paper the electrons are forced in orbital motions. Their diameter is given by the distance between slots S_2 and S_5. Scattering, however, will lead to losses in the FARADAY cages B and C.

$$i = I\mathrm{e}^{-\alpha ps} \tag{2.15}$$

$$(p_1 - p_2)\alpha s = \ln\left(\frac{I_1 i_2}{I_2 i_1}\right), \tag{2.16}$$

and for the lightest targets (hydrogen and helium), a hyperbolic dependence as pictured in Fig. 2.4, is obtained. For zero energy, the curve saturates at a certain constant level.
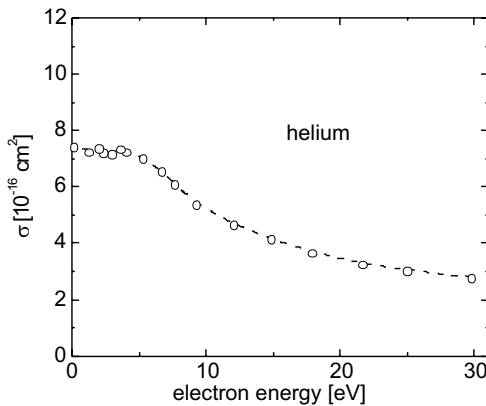
Fig. 2.4. Experimental cross sections for the elastic collision of electrons through helium as function of electron energy according to [17].

2.3.2 Differential cross section

We consider now the total cross section and the cross section of momentum transfer, which can be evaluated after having measured the angular depen-

dence of the scattering amplitude according to Eq. (2.10). It was again RAM-
SAUER (this time together with KOLLATH) who applied the measuring princi-
ple sketched in Fig. 2.5 [18]. A reactor contains a filament that emits electrons
which are accelerated across an electric field. These electrons are deflected by
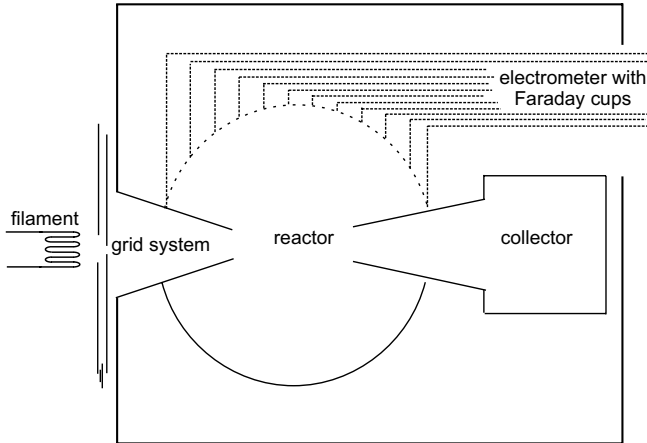gas molecules and are caught in FARADAY cages and eventually measured.

Fig. 2.5. Sketch of the apparatus developed by RAMSAUER and KOLLATH to deter-
mine the angular dependence of the cross section for elastic scattering of electrons
after [18].

Some general guidelines are:

- At sufficiently high electron energies, we find an intense zero beam: Almost
  no deflection and then a gradual decline for large scattering angles.

- Approaching low electron energies, this picture becomes more compli-
  cated. Maxima and minima occur which resemble X-ray diffractograms
  of fluids (Fig. 2.6). For the first time, this was observed by BULLARD and
  MASSEY in argon. They explained these patterns by diffraction of electron
  waves at symmetrically scattering atoms, comparable with the pattern of
  light waves which are scattered at spheres of similar dimension [19]. How-
  ever, for the quantitative interpretation of this phenomenon, a quantum
  mechanical treatise is required.

- The complexity of this pattern rises with increasing atomic number of the
  scattering atom.

For elastic scattering of electrons of low energy, a successful collision is
assumed to have occurred for a deflecting angle of 90°. According to Eq. (2.11),
ν_m then equals ν_c. For the noble gases, both dependencies (on velocity and on
angle) have been measured; hence, $\sigma_c(v)$ and $\sigma_m(v, \vartheta)$ can be compared. For low
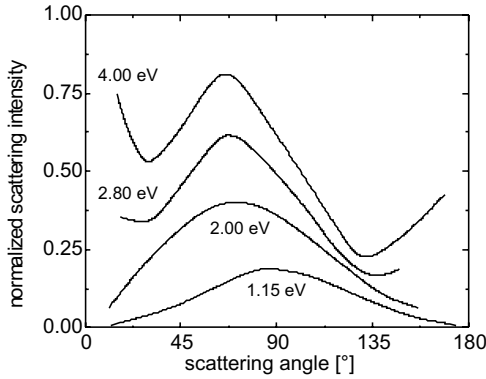
Fig. 2.6. Scattering of electrons at argon atoms for very low electron energies [20] (© J. Wiley & Sons, Inc.).

energies, the agreement is satisfactory (argon) or almost perfect (helium, Figs. 2.7).
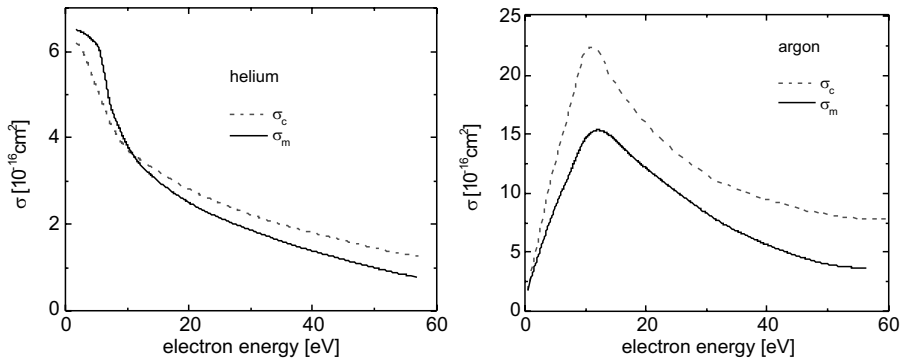

Fig. 2.7. Comparison between total cross section σ_c and cross section for momentum transfer σ_m for the lightest noble gas helium and the medium-light noble gas argon, which behaves entirely differently for low electron energies [20]. For helium, σ_m exceeds σ_c for low electron energies: The scattering in the backward direction becomes more important than forward scattering.

2.3.3 Modeling

2.3.3.1 Cross section for the interaction between a point charge and an induced dipole. For potentials which decrease with r^{-4} (i. e. for forces which decline with r^{-5}), there exists a simple correlation between the frequency of collisions and number density, which was pointed out by MAXWELL [21].

An electron is moving in a field of a potential Φ which declines with r^{-n} (Fig. 2.2). Introducing polar coordinates yields

$$v^2 = v_{\parallel}^2 + v_{\perp}^2 = \left(\frac{\partial r}{\partial t}\right)^2 + r^2 \left(\frac{\partial \phi}{\partial t}\right)^2, \tag{2.17}$$

with $v_{\parallel}$ and $v_{\perp}$ the two components of the velocity $\boldsymbol{v}$ which are orientated in parallel or in perpendicular fashion with respect to the radius vector $\boldsymbol{r}$, we find for energy and angular momentum

$$E = \frac{m_0 v^2}{2} + \Phi = \frac{m_0}{2} \cdot \left[\left(\frac{\partial r}{\partial t}\right)^2 + r^2 \left(\frac{\partial \phi^2}{\partial t}\right)\right] + \Phi = \text{const}, \tag{2.18}$$

$$L = m_0 r^2 \frac{\partial \phi}{\partial t} = \text{const}. \tag{2.19}$$

With b the scattering parameter, the distance between the two particles under consideration (for lacking interaction, the trajectory of the electron would be a straight line) we get for the angular momentum

$$m_0 r^2 \frac{\partial \phi}{\partial t} = m_0 b v_0, \tag{2.20}$$

with the boundary condition for the initial energy E_0 (initial velocity v_0) for vanishing potential $\Phi = 0$

$$E_0 = \frac{m_0 v_0^2}{2}. \tag{2.21}$$

Since the time-dependent derivations of the coordinates are

$$\frac{\partial \phi}{\partial t} = v_0 b r^2 \wedge \frac{\partial r}{\partial t} = \frac{\partial r}{\partial \phi} \cdot \frac{\partial \phi}{\partial t} = \frac{\partial r}{\partial \phi} \cdot v_0 b r^2, \tag{2.22}$$

we obtain

$$\frac{\left(\frac{\partial r}{\partial \phi}\right)^2 E_0 b^2}{r^4} + \frac{E_0 b^2}{r^2} + \Phi = E_0. \tag{2.23}$$

From Eq. (2.23), the angular dependence of r ($\partial r / \partial \phi$) yields

$$\frac{\partial r}{\partial \phi} = \pm \frac{r^2}{b} \left(1 - \frac{b^2}{r^2} - \frac{\Phi}{E_0}\right)^{1/2}, \tag{2.24}$$

with the minus sign for approaching particles, the plus sign for disappearing ones. This function exhibits a minimum at $\partial r / \partial \phi = 0$, when the argument of the square root vanishes. With $\Phi = ar^{-n}$ and $b = cr$, we find for the minimum distance $r_{\min}$

$$r_{\min}^n = \frac{2a}{m_0 v_0^2 (1 - c^2)}. \tag{2.25}$$

Applying the hard sphere model, the minimum distance $r_{\min}$ equals to $\sigma_{\text{scatt}} = \pi r_{\min}^2$, and we can write it down with combined constants:

$$\sigma_{\text{scatt}} = \frac{A}{v^{4/n}}. \tag{2.26}$$

For $n = 4$, this yields the simple form

$$\sigma_{\text{scatt}} = \frac{A}{v}, \tag{2.27}$$

which is the potential which will form between a point charge and an induced dipole with moment μ_{ind} (with α the polarizability):

$$\mu_{\text{ind}} = \alpha E \wedge E_{\text{pot}} = -\frac{1}{2}\mu \cdot E = -\frac{1}{2}\alpha E^2. \tag{2.28}$$

For a COULOMB potential, we calculate the potential energy to

$$E_{\text{pot}} = -\frac{1}{2}\alpha\frac{e_0^2}{r^4}. \tag{2.29}$$

With this derivation, we have obtained the important result that for a force with a declining behavior according to r^{-5}, e. g. a point charge in a neutral gas which exerts polarization effects, the specific conduct of the $\mathcal{EEDF}$ (and hence v_{e}) does not matter at all. In this very special case, the frequency of elastic collision between electrons and neutrals ν_{m} (and also the mean free path λ) will become a single function of the number density [21].[1] σ will then scale with $1/v \propto 1/\sqrt{E_{\text{kin}}}$ (Fig. 2.8).
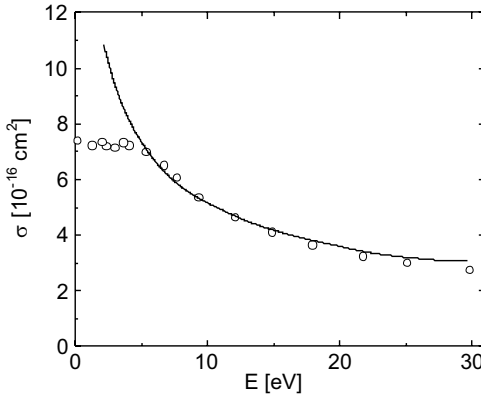
Fig. 2.8. Experimental and calculated cross sections for the elastic collision of electrons through helium as a function of electron kinetic energy according to [17].

---

[1]For the interaction between point charges COULOMB's law holds: The potential drops according to $1/r^{n=1}$. In this case, $\sigma_{\text{scatt}} = A/v^4$, which determines the generalized resistance η in the case of high-density plasmas (cf. Sect. 14.7.2).

2.3.3.2 Ramsauer effect. For electron energies larger than some tens V, the cross section decreases gradually; it scales with the inverted ionization potential and is proportional to the polarizability (to a first order approximation: the atomic number) since scattering takes place at the bound electrons of the atoms. Very low values of the scattering cross section are caused by weak interaction with the higher noble gas atoms (RAMSAUER effect, Fig. 2.7.2 [22]). This effect was explained for the first time using quantum mechanical methods by ALLIS and MORSE using the partial wave method.

According to this theory, the cross section of elastic scattering is composed of partial cross sections, which are denoted s scattering for $l = 0$, p scattering for $l = 1$ etc. (η_l is the partial phase shift of the waves with angular momentum $L = \sqrt{l(l+1)}\hbar$, $p = \hbar k$):

$$\sigma_0 = \sum_l \sigma_l \wedge \sigma_l = \frac{4\pi}{k^2}(2l+1)\sin^2\eta_l. \tag{2.30.1}$$

The affiliated potentials become deeper but simultaneously more short-ranged— the atomic radius grows by about 150 % when going from helium (0.49 Å) to xenon (1.24 Å) leading to a ratio of atomic volumes of about 16, whereas the number of electrons increases by a factor of 27! For slow electrons ($k \to 0 \wedge \lambda \to \infty$), L becomes very small, and for the noble gas atoms argon and heavier, only the component of zero order, i. e. s scattering, remains of importance:

$$\sigma_0 = \frac{4\pi}{k^2}\sin^2\eta_0. \tag{2.30.2}$$

$\eta_0 \to \pi$ at $k \neq 0 \Rightarrow \sigma_0 = 0$. Hence, a head-on collision ($\vartheta = \pi$) between an electron and an atom cannot be observed. For the heaviest noble gas atoms (Xe and Rn) this effect is much more distinct than for the lighter ones (Ar and Kr) and vanishes for He and Ne.

2.3.4 The frequency of elastic collisions between electrons and neutrals

For the special cases of hydrogen and helium, the collision frequency simply scales with discharge pressure (number density): $\nu_m = \text{const} \times p_0$, which follow the equation with $p_0 = 273/T \times p$ [p in Torr (in Pa), Figs. 2.9]:

- He: $\nu_m = 2.31 \times 10^9 p_0$ ($3.07 \times 10^{11} p_0$);

- H$_2$: $\nu_m = 5.93 \times 10^9 p_0$ ($7.89 \times 10^{11} p_0$).

This does not hold true for the heavier noble gases (at least for neon, we see a fairly good approximation with an asymptotic behavior) and a strange conduct is observed for chlorine. Here, the maximum is foreshadowed by a minimum at very low energies in Cl· and Cl$_2$ (Fig. 2.10).

Following MASSEY, we estimate the mean free paths for electrons λ_e in argon according to Eq. (2.7) [25]. For typical electron energies of several electronvolts, we calculate a λ_e of several centimeters (Figs. 2.11).
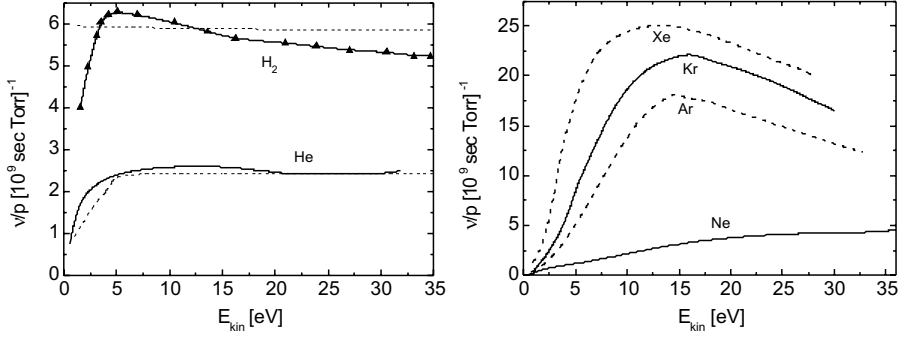
Fig. 2.9. Frequency of elastic collisions between electrons and neutrals for hydrogen and helium, and the heavier noble gases [23].
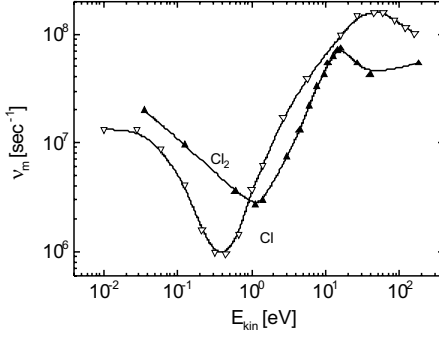

Fig. 2.10. Frequency of elastic collisions between electrons and neutrals for Cl· and Cl_2 after [24]; discharge pressure 10 mTorr.

2.3.5 Cross section and rate constant for argon

By Eqs. (2.6) + (2.11), the cross section for a specific scattering process is related to the probability of its occurrence. This frequency ν depends on the density of target molecules, and reducing ν to the unit density yields the rate constant k,

$$k = < v_e > \sigma \qquad (2.31.1)$$

in particular for the momentum transfer k_m:

$$k_m = < v_e > \sigma_{elast}. \qquad (2.31.2)$$

This relation allies atomic properties which must be evaluated by scattering experiments with macroscopic kinetic parameters, with the mean electron velocity being the connecting link. The directed energy E from the scattering experi-
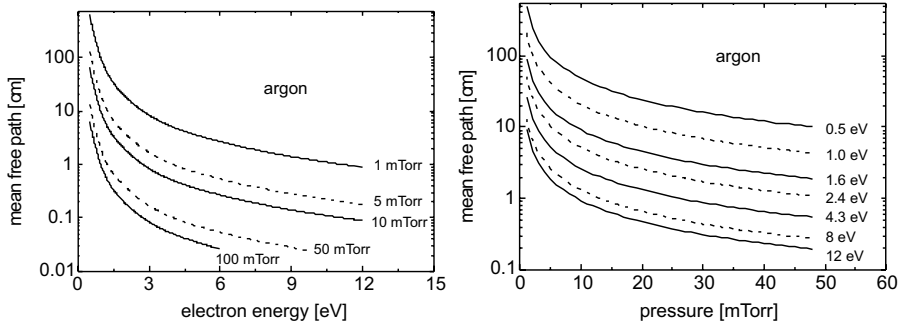
Fig. 2.11. Calculated mean free paths of low-energy electrons (below the ionization threshold) in argon after [25].

ments has to be replaced by the thermal energy E for a discharge. Most frequently, a MAXWELLian distribution is assumed but especially for low plasma densities ($E = k_B T_e$), however, this assumption has turned out to be highly questionable (Sect. 14.1). The connection between σ and k is pictured for argon in Figs. 2.12. The data for σ_{elast} have been compiled from NAKANISHI and SZMYTKOWSKI [26, 27].
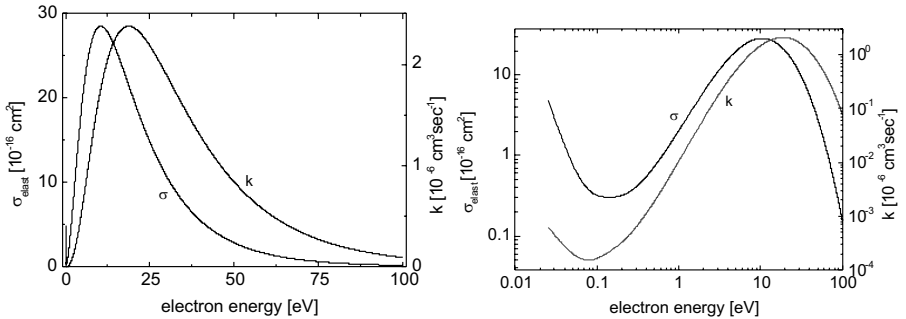
Fig. 2.12. Argon: total cross section for elastic scattering σ_{elast} and the corresponding rate constant $k = \sigma_{elast} \times <v_e>$ after [25] − [27].

2.4 Elastic collisions between heavy particles

The scattering among heavy particles exhibits a remarkably distinct maximum in the forward direction [28]. Measuring such an angular dependence is almost hopeless. For energies of a few electronvolts, the requirements for angular resolu-

tion are difficult to meet, and these demands increase with rising momentum of the projectiles. The accuracy necessary to measure the total elastic cross section for argon is for thermal atoms 0.70°, those with 1 000 K temperature require an accuracy of 0.30°, which is even sharper for atoms of 1 eV kinetic energy (11 600 K, 0.11°). These difficulties are reinforced for the measurement and calculation of the differential cross section which means the determination of the fraction of molecules which hit target molecules and are subsequently scattered into the solid angle $d\Omega = 2\pi \sin\theta d\theta$. In Table 2.1, the results of calculations for the differential cross section of helium against a beam of protons for two different scattering potentials (COULOMB and HARTREE, a simple pseudopotential) are compiled [29].

Table 2.1. Differential cross sections $d\sigma(\vartheta)/d\Omega$ per unit solid angle for protons of kinetic energy of 110 eV in helium in units of a_0^2.

$\angle$	$d\sigma(\vartheta)/d\Omega$	
	Hartree potential	*Coulomb potential*
0	9×10^3	∞
12	7.85	124.0
28	2.00	6.10
34	0.72	2.85
57	0.21	0.40
80	0.08	0.12
114	0.04	0.04
137		0.03
167		0.02

This forward direction is more distinct for larger kinetic energies of the projectiles (coming from low energies, only elastic scattering processes can occur). Normally, the determination of the angular dependence is confined to the range without the zero beam. One of the pioneering experiments was carried out by BERRY and CRAMER in neon and argon [30] − [33] (Fig. 2.13). We note that the cross section remains at several Å^2 up to kinetic energies of about 500 eV. Hence, an ion beam is almost entirely dissipated after having passed a distance of only 1 cm at high pressures (cf. Sect. 6.8).

However, some advanced, indirect methods are available, e. g. measuring the complex conductivity (Sect. 5.6), and the line width of the electron cyclotron resonance, which is mainly determined by the collisions between electrons and neutrals [34] (Sect. 7.5).
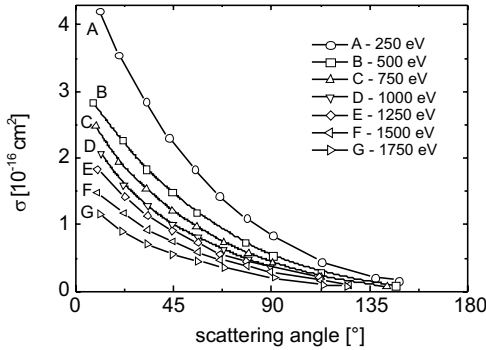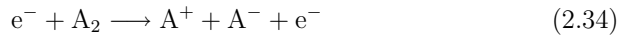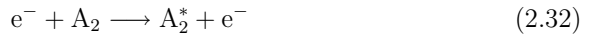
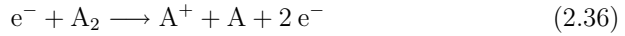**Fig. 2.13.** Cross section of Ar^+ ions in argon as a function of scattering angle [30].

2.5 Inelastic collisions

2.5.1 Inelastic collisions between electrons and heavy particles

During inelastic collisions, internal grades of freedom are excited by transformation of kinetic energy of the colliding projectiles into internal energy levels of the target. For electron impact, the most important reactions are with A^* an excited molecule:

- Excitation in upper molecular states (vibration levels or electronic states, [Eq. (2.32)].

- Dissociation into radicals (which is very effective in discharges through electronegative gases [35], [Eq. (2.33)].

- Dissociation into ions [Eq. (2.34)].

- α-ionization [Eq. (2.35)].

- Ionizing dissociation [Eq. (2.36)] and

- Electron attachment (dissociative or electron attachment, respectively), for electronegative gases [Eq. (2.37)].

$$e^- + A_2 \longrightarrow A_2^* + e^- \tag{2.32}$$

$$e^- + A_2 \longrightarrow 2\,A^* + e^- \tag{2.33}$$

$$e^- + A_2 \longrightarrow A^+ + A^- + e^- \tag{2.34}$$

$$e^- + A_2 \longrightarrow A_2^+ + 2e^- \tag{2.35}$$

$$e^- + A_2 \longrightarrow A^+ + A + 2\,e^- \tag{2.36}$$

$$e^- + A_2 \longrightarrow A^- + A^*. \tag{2.37}$$

2.5.1.1 Experimental methods. In atomic gases, dissociation reactions do not take place; one of the "classical" reaction is the ionization of mercury vapor by electron impact (FRANCK-HERTZ experiment, Figs. 2.14). In a triode tube
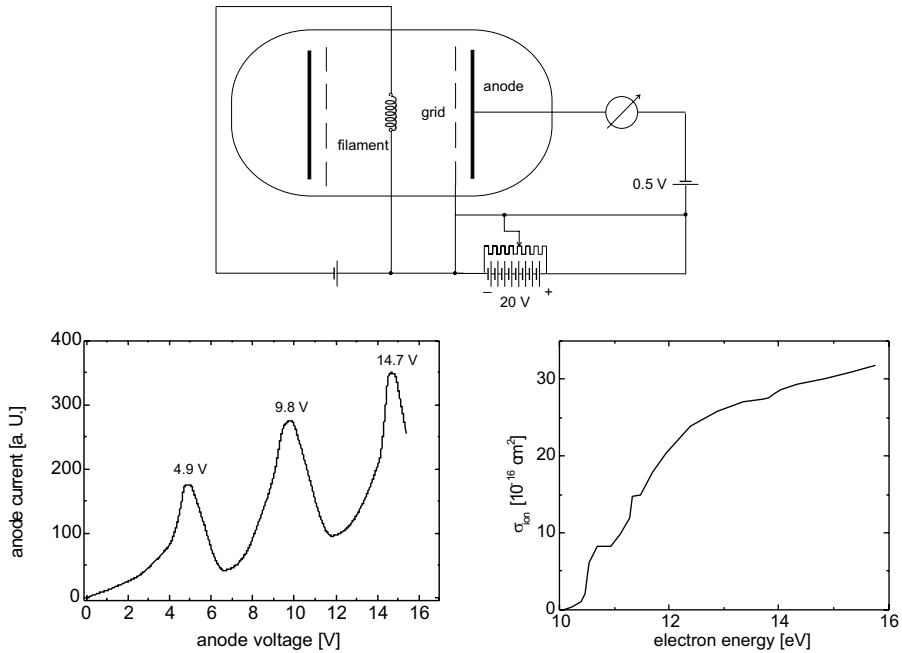

Fig. 2.14. FRANCK-HERTZ experiment. Top: experimental setup, bottom: the anodic current (LHS) and the cross section of ionization (RHS) as functions of acceleration voltage (electron energy) in mercury vapor [36]. At the ionization potential of 4.9 eV and its multiples, the characteristic exhibits distinct deviations from the expected behavior, and the cross section does not exhibit a smooth behavior [37].

filled with mercury vapor, the electrons which are emitted by a glowing cathode are accelerated through a uniform field to a grid with the anode plate placed directly behind the grid. Those which have passed it will be slowly decelerated by elastic collisions with gas atoms, but in general, we observe a slight increase of the anodic current with growing anodic voltage. However, when the ionization potential of mercury (4.9 eV) has been reached, the $I(V)$ characteristic

drops sharply. This phenomenon is caused by inelastic collisions of the electrons with mercury atoms which are ionized by electron impact. A small retarding field between grid and anode causes the anodic current to vanish at this value, because the electrons have less than 4.9 eV kinetic energy and are not able to move against this retarding potential:

$$\mathrm{Hg_{vapor}} + \mathrm{e}^- \longrightarrow \mathrm{Hg}^+ + 2\,\mathrm{e}^-. \tag{2.38}$$
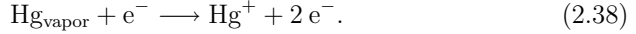
This setup has been improved by MAIER-LEIBNITZ [38] and further by SCHULZ and FOX who employed a retarding potential difference method [39]. They concluded that the electron energy distribution function, $\mathcal{EEDF}$, in the original FRANK-HERTZ experiment was very broad, too broad to obtain an accurate measurement of the excitation probability. For that purpose, the energy of the bombarding electrons as well as the energy of those that have lost energy in inelastic collisions must be known. Therefore, they constructed an energy filter system which made use of also in the determination of the ion energy distribution function $\mathcal{IEDF}$ (cf. Chap. 6). By means of this three-grid optics, it is possible to extract a nearly monoenergetic beam of electrons (Figs. 2.15).
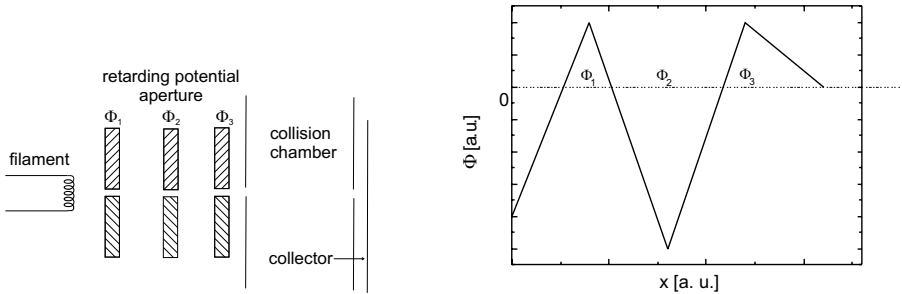

Fig. 2.15. By employing the retarding potential difference method, SCHULZ and FOX could significantly improve the accuracy of the determination of the inelastic scattering cross section [39].

The first grid is positively biased by approximately 3 V with respect to the filament and serves to draw electrons. The second grid is slightly negative with respect to the filament, the electrons must run uphill against a retarding potential, and as a result, the $\mathcal{EEDF}$ is chopped off. It is only the high-energy fraction of the electrons which is able to pass. The third grid shows the same potential as the first grid. Since the $\mathcal{EEDF}$ can be sensitively influenced by variation of Φ_2, $\Phi_2 + \Delta\Phi_2$, we obtain two values for the collector current which can be solely referred to the electrons with energy $\Delta\Phi_2$. By variation of the retarding potential Φ_2, grid 2 also varies the voltage to the collision chamber which determines the collector current, i. e. the $\mathcal{EEDF}$.

2.5.1.2 Cross section. The cross section for an inelastic scattering process exhibits a threshold which is followed by a steep rise (several orders of magnitude) to reach a maximum. This is sharply peaked for optical transitions at energies which are close to the threshold, and a little broader for ionizations at about $100 - 150$ eV, which is consistent with the DE BROGLIE wavelength of the electrons of approximately 1 Å, the typical diameter of the targets where the electron waves are expected to be deflected most intensely. For higher energies, we find a slow decrease since the time of interaction between the collision partners is gradually shortened (Fig. 2.16 in linear scale, Figs. 2.17 in logarithmic scale).
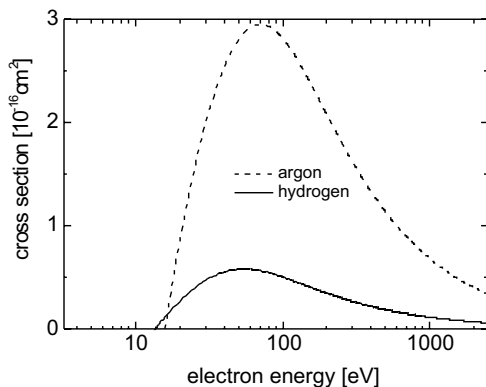
Fig. 2.16. Typical energy dependence of the cross section for inelastic scattering between electrons and molecules for argon and hydrogen.

The cross section of ionization has been comprehensively described by BETHE and SALPETER [40, 41]. According to BORN's approximation, the total cross section of a discrete excitement into state n with energy E_n of the excited state can be approximated by

$$\sigma_n = \frac{4\pi a_0^2 z^2}{T} \left[A \ln(4\,B\,T) + \frac{C}{T} + O\left(\frac{1}{T^2}\right) \right], \tag{2.39}$$

with a_0 BOHR's radius, z the charge and T the kinetic energy of the projectile, mostly given in Rydberg ($= 13.6$ eV), irrespective of the nature of the projectile. A is the squared matrix element of the specific excitation, and the B, C are constants which will be generated during the integration [42], and the factor 4 in the logarithmic summand which is left for historical reasons. The third term is a very small correction, and most frequently, the second term is neglected as well, and we arrive at the following simplified approximation [43, 44], which is known as BETHE's asymptotic cross section [41]:

$$\sigma_n = \frac{4\pi a_0^2 z^2}{T} \left[A \ln(4\,B\,T) \right]. \tag{2.40}$$

Unfortunately, this theory holds best for large kinetic energies of the projectiles. However, for ionization and excitation processes by electron impact, the energy

dependence just above threshold is of extreme importance. To describe this regime properly, in particular the steep rise beyond threshold and the maximum, WANNIER developed a theory for single ionization which states that in the energy range near threshold, the probability of ionization rises exponentially with the energy in excess of the ionization energy (more correctly: raised to the 1.127th power) [45, 46], which had been improved by GELTMAN [47]. LOTZ introduced an equation with three parameters (a, b and c), which approximates the cross sections of most of the interesting gases within a deviation of less than $\pm 10\%$ to experimental data [44] (Fig. 2.17.2):

$$\sigma_n = a \, \frac{\ln(T/E_n)}{T} \left\{ 1 - b \, \exp\left[-c \left(\frac{T}{E_n} - 1 \right) \right] \right\}. \tag{2.41}$$
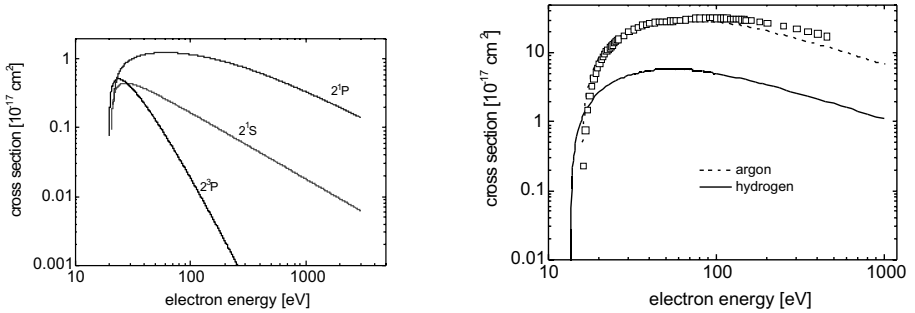
Fig. 2.17. Typical dependence of the inelastic cross section of molecules and electrons on the electronic kinetic energy. Note the double logarithmic scale to make the steep increase visible. LHS: energy dependence of the cross section for excitation into various optical levels of helium, according to the formula of MITYUREVA and SMIRNOV [48]. RHS: LOTZ's theory for ionization of hydrogen and argon, experimental data for argon are from one of the most cited papers by RAPP and ENGLANDER-GOLDEN [49].

The main difference between ionization and excitation into optical levels by electron impact is caused by the electrostatic interaction of three charges after the collision process. For the first time, this problem has been addressed by WANNIER ([46], also cf. [50], Fig. 2.17.1). As a main result, the maximum for excitation into optical levels is located very close to the threshold, whereas for ionization, the difference in energy between maximum and threshold will be no less than a factor of 4 in excess of the ionization energy [48]. The graphs of Figs. 2.17.1 are plotted applying an approximation containing three adjustable parameters σ_0, ϕ, and γ:

$$\sigma_n = \sigma_0 \sqrt{\frac{T - E_n}{T}} \left(\frac{T}{E_n} - 1 + \phi \right)^{-\gamma}. \tag{2.42}$$

In summary, we find the cross section for ionization by electronic impact to rise sharply from zero at a specific threshold by several orders of magnitude until it reaches a maximum at approximately 100 eV because the DE BROGLIE wavelength of about 1.2 Å fits the atomic dimensions. For further increases of electron energies, the cross section gradually decreases. At 500 eV, it has typically weakened by a factor of about 2 compared with its maximum value (Fig. 2.18).
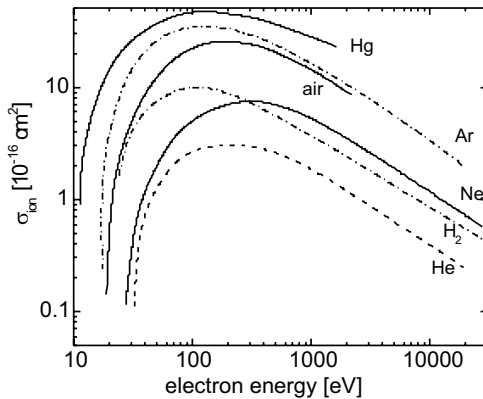

Fig. 2.18. Cross section for ionization by electron impact for various gases in double-log-arithmic scale [51] (© Oxford University Press).

2.5.1.3 Rate constant for ionization. Employing Eqs. (2.31), we ally the frequency of ionization with the rate constant for this process, pictured in Figs. 2.19 for ionization of argon, with a MAXWELLian distribution assumed. In fact, it is the rate constant we are interested in to calculate the carrier generation. Especially at the threshold, the slope of the $k(E)$ curve repeats the steep increase of the cross section. In low temperature plasmas, it is but these electrons in the high-energy tail that are responsible for the maintenance of the discharge.

2.5.1.4 Electron attachment. Electron attachment plays a significant role in discharges through electronegative gases. One of the main processes is dissociative electron attachment, e. g.:

$$O_2 + e^- \longrightarrow O^- + O, \tag{2.43}$$

$$SF_6 + e^- \longrightarrow SF_5^- + F, \tag{2.44}$$

a two-body collision leading to the formation of a negatively charged oxygen ion and and oxygen atom, or a very special case, the formation of a SF_5^- ion and a fluorine atom.[2]

---

[2]It is this ion which captures almost all the electrons at very low discharge pressures.
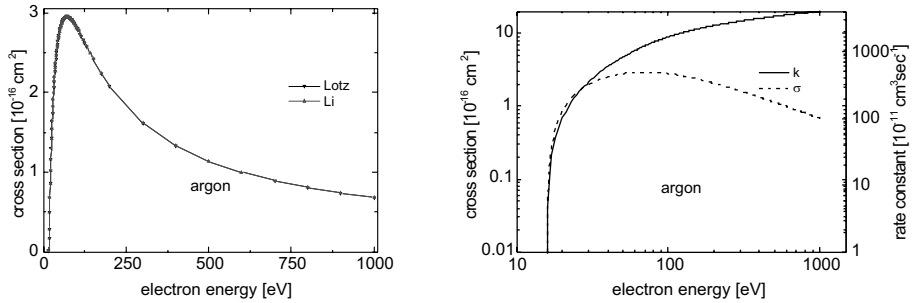
Fig. 2.19. Ionization by electron impact for argon. LHS: Two different formulae, according to LOTZ and LI, yield an almost indistinguishable result [44, 52]. RHS: For cross section and rate constant, a MAXWELLian distribution for the electrons assumed. The calculation is based on the LOTZ formula [44].
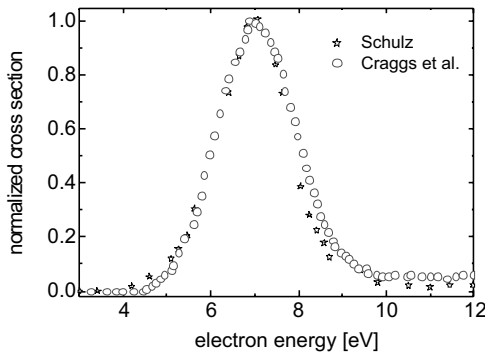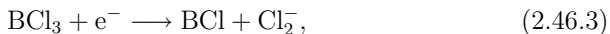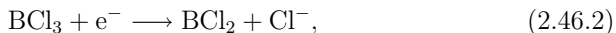

Fig. 2.20. Normalized cross section of electron attachment and formation of O^- ions. The asterisks were evaluated by SCHULZ, the circles are due to measurements by CRAGGS *et al.* The maximum (SCHULZ) has been found at 1.25×10^{-18} cm^2 and 6.7 eV [53] (© J. Wiley & Sons, Inc.).

Atoms are not able to capture electrons in a two-body collision process because the laws of conservation of momentum are violated. Therefore, the cross sections are very low (in the order of 10^{-18} cm^2), but exhibit sharp maxima at electron energies of a few eV (Fig. 2.20). The density of negative ions can far surpass that of the electrons which changes the characteristics of the discharge completely.

As is evident from Fig. 2.22, the cross section for dissociative attachment exhibits two maxima for oxygen. The first can be referred to reaction (2.43), whereas the maximum at higher energies is due to the reaction

$$e^- + O_2 \longrightarrow O^- + O^+ + e^-. \tag{2.45}$$
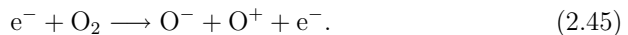
One of the most prominent cases is that of BCl_3 as an additive in discharges through chlorine. In principle, three reaction paths are possible [54]:

$$BCl_3 + e^- \longrightarrow BCl_3^*, \tag{2.46.1}$$

$$BCl_3 + e^- \longrightarrow BCl_2 + Cl^-, \tag{2.46.2}$$

$$BCl_3 + e^- \longrightarrow BCl + Cl_2^-, \tag{2.46.3}$$

with BCl_3^* the metastable parent anion, which can be effectively generated by extremely low energy electrons up to 0.1 eV [54]. Although the pyramidal BCl_3^- ion is expected to be long lived, (PETROVIC *et al.* detected this anion in a mass spectrometer, which indicates a lifetime in the microsecond range [55]), due to its small electron affinity of 0.33 eV, it will be easily discharged by electron impact. All of the discharges which are dealt with in the following chapters exhibit higher mean electron energies. Therefore, BCl_3^- anions are most likely to elude detection.[3] TAV *et al.* have estimated the cross section for dissociative electron attachment to BCl_3 to be $\leq 5 \times 10^{-18}$ cm^2 [according to Eqs. (2.46.2) and (2.46.3)] and for electron attachment to BCl_3 according to Eq. (2.46.1) to 4.5×10^{-15} cm^2.

2.5.1.5 Total collision cross section. Since the numerous possibilites of excitation exclude each other, their probabilities must be added up, and we can define a total cross section for all possible excitations [57]:

$$\sigma_{\text{tot}} = \sum_i P_i \sigma_i(v), \tag{2.47}$$

with P_i the probability and σ_i the differential cross section for reaction i. For example, the maximum of the total cross section for electron impact for argon amounts to 26×10^{-16} cm^2 = 26 Å^2 and can be found just above the ionization threshold of 15.76 eV. This means an electronic mean free path of 1.5 mm at a discharge pressure of 50 mTorr (7 Pa, $n = 2 \times 10^{15}$ cm^{-3}). For low electron energies, the cross section for elastic scattering almost equals the total scattering cross section since the velocities of the electrons do not suffice for atomic or molecular excitation. Especially for the noble gases, numerous measurements have been performed and modeled. A compilation of these measurements is pictured in Fig. 2.21.

It was MYERS who split up the total cross section $\sigma_{O_2,\text{tot}}$ into its separate parts for oxygen (Fig. 2.22) [58]. For energies up to approximately 50 eV, the

---

[3]However, GOTTSCHO and GAEDE succeeded in generating and observing this anion in low-frequency discharges at 50 kHz where the electron density will completely relax during each half cycle leaving ample time for the slow electrons to generate the BCl_3^- anion [56]. Using a non-invasive method (laser photodetachment), they could detect this anion before the electrons were reheated in the next half cycle.
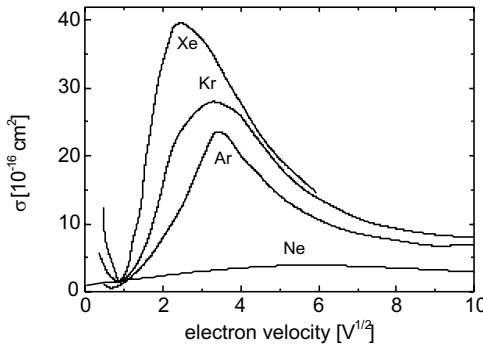
Fig. 2.21. Experimental scattering total cross sections of the heavy noble gases for low electron velocities. The almost complete transparency at very low velocites is striking; the distinct maximum corresponds well with the ionization energy E_{ion} [25] (© Oxford University Press). Compare with Fig. 2.7.2.

cross section for elastic scattering is the most important contribution to the cross section for ionization.
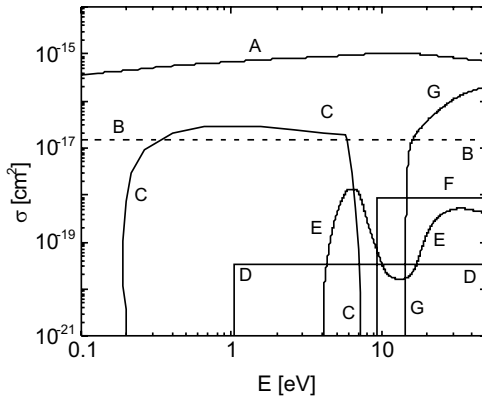

Fig. 2.22. The single contributions of the total cross section for electronic impact were split up by MYERS for O_2 [58]. The letters denote the contributions as follows: A: elastic scattering, B: rotatory excitation, C: oscillatory excitation, D: excitation to singlet-oxygen, E: dissociative attachment (two maxima!), F: excitation to upper electronic states, G: ionization.

2.5.2 Inelastic collisions between heavy particles

To begin with, the literature covering the low-energy range, which is of paramount importance in glow discharges, is widely scattered, in particular when we compare this range with the countless number of papers dealing with energies exceeding 1 keV. This is mainly caused by the low cross sections for inelastic processes. Hence, elastic scattering will still dominate the interaction between the gas constituents. The main reactions between heavy particles are:

- Generation of electrons by ionic impact [so-called β-ionization, Fig. 2.23, Eq. (2.48)].

- Excitation to electronic levels [Eq. (2.49)].

- Electron stripping [Eq. (2.50)].

- Simple charge transfer [Figs. 2.25 − 2.28, Eq. (2.51)].

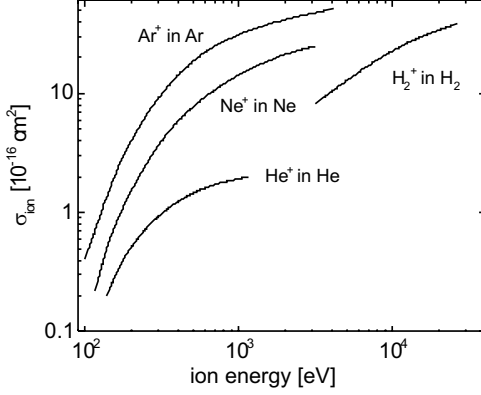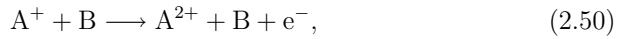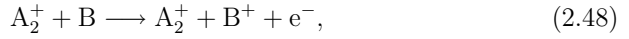- Double charge transfer [Eq. (2.52)].

Fig. 2.23. β-ionization: cross section of ionization by ions of the parent gas after [59]. The values are not corrected by ionizations caused by secondary electrons (© Oxford University Press).

$$A_2^+ + B \longrightarrow A_2^+ + B^+ + e^-, \tag{2.48}$$

$$A^{+,*} + B \longrightarrow A^+ + B^*, \tag{2.49}$$

$$A^+ + B \longrightarrow A^{2+} + B + e^-, \tag{2.50}$$

$$B^+ + A \longrightarrow A^+ + B, \tag{2.51}$$

$$A^+ + B \longrightarrow A^- + B^{2+}. \tag{2.52}$$

As we can see from Fig. 2.23, the threshold for ionization by ionic impact is relatively low but amounts to about twice the ionization potential. The classical theory of J.J. THOMSON yields cross sections equal in size for equal velocities of ions and electrons. The same result is obtained with quantum mechanics with the restriction that the impact of the colliding particles is large compared with their pair potential (BORN's approximation). Choosing the abscissa scale skilfully (in fact, it is the momentum of the colliding particle), we can find a similar behavior between the ionic and the electronic cross section, however, dilated by some orders of magnitude for the heavy particles (Fig. 2.24). The
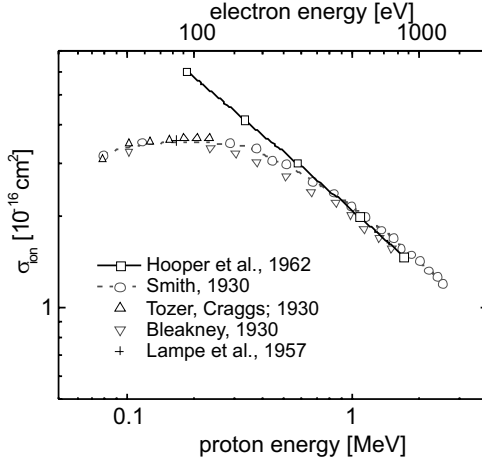
Fig. 2.24. Comparison of the ionization cross sections of argon for protons (dashed) and electrons (solid) [60] (© J. Wiley & Sons, Inc.).

cross sections for ionization (β-ionization) do not reach hogh values until the ions have been accelerated to velocities which are comparable to those of the electrons for α-ionization. Hence, for energies up to several hundreds of eV, the ionic cross section is smaller by about two orders of magnitude. For the same kinetic energy, the ionic momentum is considerably greater, which leads to very short DE-BROGLIE wavelengths. Hence, even for inelastic collisions, there are hardly any diffraction effects.

2.5.2.1 Charge transfer. For charge transfer, an almost complete exchange of momentum is of importance. Consider a rapidly moving ion colliding with a slow molecule (Fig. 2.25). This collision can result in a slowly moving ion and a rapid neutral, and the components of velocity are conserved. In the case that both colliding particles have the same mass, this process is very efficient, and this collision is denoted (*symmetric or resonant charge transfer,* Fig. 2.26). We expect the cross section for this process to be comparable with that for elastic collision.

To begin with, we assume A $\neq$ B, *i. e.* the ionization potentials should be differ by the amount ΔE_{ion}:

$$E_{\mathrm{ion,B}} = E_{\mathrm{ion,A}} + \Delta E_{\mathrm{ion}}. \tag{2.53}$$

MASSEY discussed this charge transfer by means of the correspondence principle [62].

For a particle velocity v smaller than that of the bounded electrons, they will adapt to this disturbance without an electron transfer (so-called adabatic approximation). We find the time of collision τ to scale inversely with the frequency ν of an electron oscillation with $\tau \approx b/v$ (b the so-called adiabatic parameter):
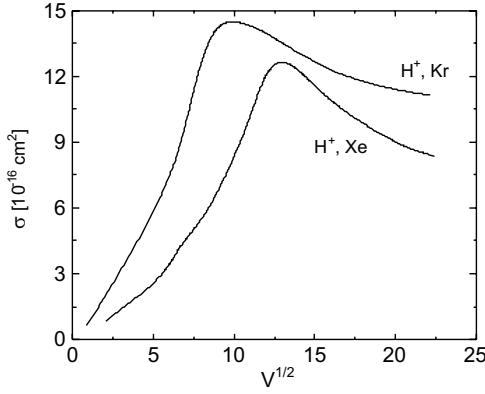
Fig. 2.25. Cross section for the asymmetric charge transfer of protons in noble gases after [61].

$$\tau = \frac{a}{v} = \frac{1}{\nu} \wedge \nu = \frac{\Delta E_{\text{ion}}}{h} \implies v = \frac{a \Delta E_{\text{ion}}}{h}. \tag{2.54}$$

When the velocity of the particles exceeds this threshold, no adiabatic collision will take place but an ionization will occur. The larger the difference in ionization potential ΔE_{ion}, the higher the energetic threshold to become a competitive process. On the other hand, the time for interaction declines with rising energy which eventually reduces the probability of ionization: A maximum has been evolved (Fig. 2.26).
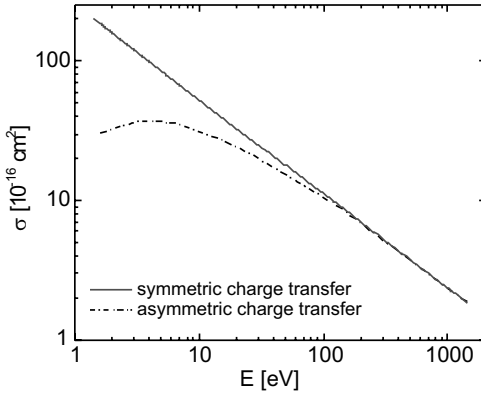

Fig. 2.26. Principal energy dependence of the two mechanisms for charge transfer. in double-logarithmic scale, the resonant charge transfer linearly scales with energy, whereas the asymmetric charge transfer exhibits an energetic maximum.

2.5.2.2 Resonant charge transfer. For a resonant charge transfer with $\Delta E_{\text{ion}} = 0$, we expect a monotonous increase in the cross section for ionization for lower energies in the adiabatic approximation. Albeit the correspondence principle predicts this conduct qualitatively correctly, more extensive descriptions of the height of the maximum (e. g. $\Delta E_{\text{ion}}/E_{\text{kin}}$) are definitely impossible.

The principal shape of the energetic dependence of the cross section is depicted in Fig. 2.26. It can be described by the formula

$$\sigma = (a - b \ln v)^2 \tag{2.55}$$

with a, b empirical constants and v the relative velocity of the colliding particles [63]. For a resonant reaction, there exists a linear relation between the cross section and the logarithmic kinetic energy (Fig. 2.27).
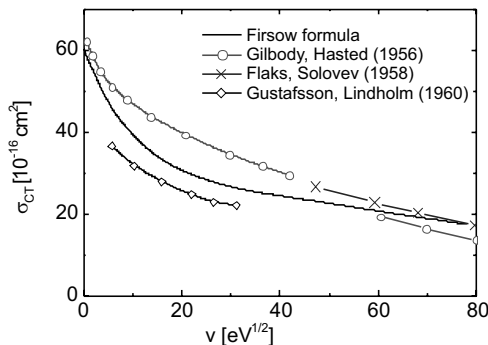

Fig. 2.27. Resonant charge transfer: $Ar^+_{fast} + Ar_{slow} \longrightarrow Ar^+_{slow} + Ar_{fast}$; comparison of experimental data with theory (Firsow formula) [64] (© J. Wiley & Sons, Inc.).

The cross section reaches a maximum for an ion in its parent gas at slow velocities. In this energy range, it can deliver the main contribution to the total cross section (Fig. 2.28). The electron transfer mostly happens without any exchange of momentum: The generated ions exhibit negligible velocities, and the scattered atoms alter their direction only in a very narrow scale; hence, the scattering cone exhibits a very low opening angle [65].

The measuring of the charge transfer was made possible by an apparatus which consists of a magnetic field which deflects the ion beam and focuses it on to the sample. To prevent multiple ionizations, the cross section of the reactor has to be made sufficiently thin. The ions produced are sucked off by an electric field which is directed perpendicular to the reactor. The ions are measured by a Faraday cage which is negatively biased to avoid distortions by secondary electrons (so-called condensor method) [66].

Ternary collisions occur relatively rarely; the ratio of the probabilities of a two-body collision over a three-body collision is about thousand [67], therefore reactions

$$2A^+ + B \longrightarrow A_2^+ + B^+ \tag{2.56}$$

(recombination) are not very likely to happen. Since the number of collisions scales with the squared pressure p (at constant temperature: With the squared number density n), the probability for recombination increases with rising pressure (cf. Sect. 4.7).
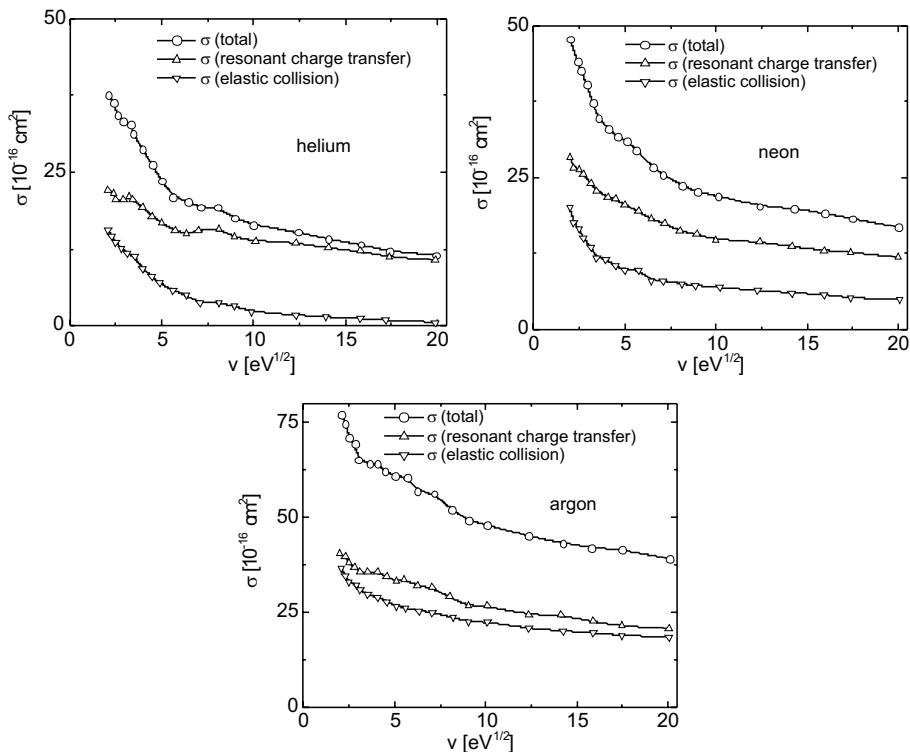
Fig. 2.28. Cross sections for the processes of elastic scattering and symmetric (resonant) charge transfer of He$^+$ in He, Ne$^+$ in Ne, Ar$^+$ in Ar [31] − [33]. At low energies, the resonant charge transfer can deliver the main contribution to the total cross section.

2.5.2.3 Penning ionization. Among the numerous reactions which can occur between heavy particles, we should mention the PENNING ionization, collisions of second order. This mechanism becomes important in discharges of reactive gases which are doped with noble gases (cf. Sects. 10.4.3, 10.6.4 and 11.8.6) and consists of ionization by metastable species.

For ionization by collisional impact, the metastable level must be higher than the ionization potential of the neutral molecule or atom. Since the return to the ground level from a metastable level is forbidden by selection rules, these levels exhibit considerable lifetimes. The metastable levels for neon (16.62 and 16.7 eV) and those of argon (11.55 and 11.72 eV) are higher than the ionization potentials of most of the gaseous elements and gaseous compounds. By doping a discharge of argon with neon, metastable neon atoms can ionize argon

atoms. The state of metastability is denoted with an asterisk (cf. also Fig. 4.4, enlargement of α).

$$\mathrm{Ne}^* + \mathrm{Ar} \longrightarrow \mathrm{Ne} + \mathrm{Ar}^+ + \mathrm{e}^-. \tag{2.57}$$
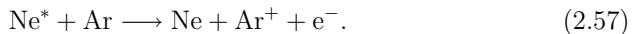
The cross sections at thermal energies are somewhat larger than the gas kinetic cross sections ($\approx 10^{-15}\,\mathrm{cm}^2$), therefore, its probability approaches unity, and this process becomes dominant very quickly [68, 69] and will be manifested in a rise of the discharge current [70].

MIERDEL discussed consecutive staircase processes which cause an additional ionization after a collision of two metastables [71]; this effect would become more probable with rising density of the metastable atoms.

$$\mathrm{Ar}^* + \mathrm{Ar}^* \longrightarrow \mathrm{Ar}^+ + \mathrm{Ar} + \mathrm{e}^-. \tag{2.58}$$
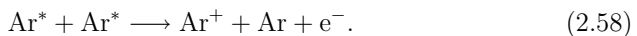
Furthermore, ionization of metastables can happen by electron impact:

$$\mathrm{Ar}^* + \mathrm{e}^- \longrightarrow \mathrm{Ar}^+ + 2\,\mathrm{e}^-. \tag{2.59}$$
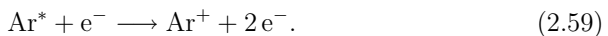
Since the energy difference from the metastable level to ionization has shrunk from 15.76 eV to only 4.21 eV, considerably more electrons are able to succeed in an ionization. Although the density of the metastable species is very low, INGOLD has estimated this mechanism to be the most important ionization source in discharges of Hg/Ar [72].

2.5.3 Collisions between photons and molecules

As final collision processes between individual particles, we must consider impacts of photons (Fig. 2.29). Again, the threshold of ionization has to be exceeded. But, in contrast to the impacts of charged particles, we observe for photons the occurrence of a steep absorption edge of several orders of magnitude at $E = E_{\mathrm{ion}}$ to decline precipitously beyond this sharp maximum. For example, the maximum of the photoelectric excitation is found for argon at 15.5 eV and exhibits a value of about $0.36 \times 10^{-16}\,\mathrm{cm}^2$.

Hence, the maxima for the yield of ionization for electrons, ions and photons are located at very different values.

2.6 Generation of secondary electrons at surfaces

2.6.1 Electrons

The impact of electrons incident on a surface causes the following reactions:

- Elastic scattering, the energy does not change but the momentum, very high contribution in the spectrum.
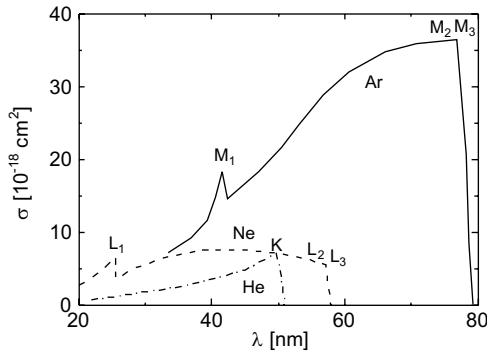
Fig. 2.29. Cross section for photo absorptions of noble gases [73] (© Springer-Verlag).

- Inelastic scattering, both energy and momentum are changed, small contribution in the spectrum.

- Towards low energies, the second rise peaking at energies between 5 and 10 eV is caused by secondary electrons (Fig. 2.30).
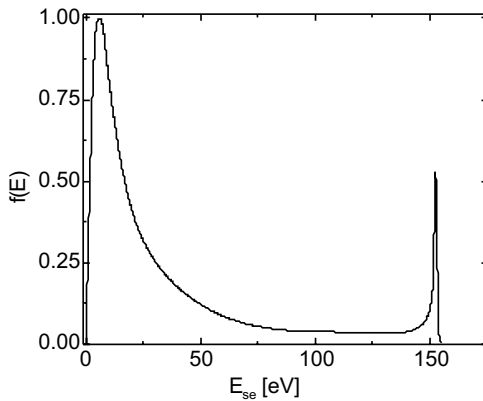

Fig. 2.30. Energy distribution of secondary electrons, $f(E)_{\mathrm{se}}$, for 160 eV electrons incident on a shiny gold surface (normalized to the low-energy maximum) [74] (© Oxford University Press).

The yield of secondary electrons depends sensitively on

- The energy of the electrons incident on the surface, which causes a maximum at medium energies. At low energies, the electrons are rather absorbed, at higher energies, they are scattered elastically.

- The chemical composition of the topmost layer: It rises with increasing density and work function with the well-known periodic dependencies. The yield increases with growing fill-up of the electronic shells. When the filling of a new shell has begun before an inner shell has been completely filled, we observed discontinuities, in particular for half-occupied shells.

- The quality of the surface: the shinier, the higher the yield.

For many metals with a clean surface the yield for secondary electrons, δ, equals unity (Fig. 2.31). For insulating layers, the values for δ can reach 15 (to measure δ, momentum methods are applied, however, the errors are rather large).
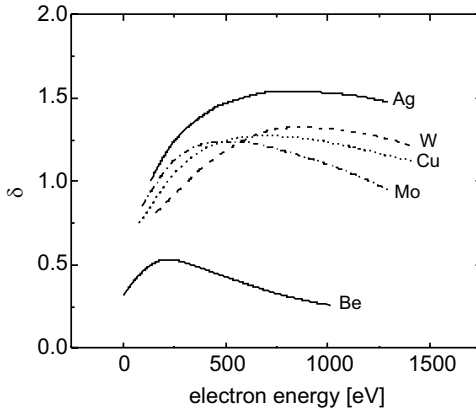

Fig. 2.31. Coefficients for secondary emission, δ, for several metals as a function of the energy of the primary electrons incident on the surface.

In insulating materials, the conduction band lacks electrons almost entirely whereas the valence band is nearly filled. Hence, the primary electrons can generate secondary electrons only by interaction with valence band electrons. But these electrons gain a higher amount of kinetic energy than comparable metal electrons, which enhances their probability of reaching the surface and eventually leaving the substrate. For the same reason, the yield increases with flatter angles of incidence.

To differentiate between the electrons, the coefficient for backscattering η refers to those electrons with energy between 50 eV and the energy of the electrons incident on the surface, and the coefficient for secondary electrons δ refers to those electrons having energy between 0 and 50 eV.

2.6.2 Ions

Ions incident on the surface can release electrons as well, and this mechanism is of considerable importance in DC discharges and also plays a role in RF discharges which are capacitively coupled. The energy distribution of the secondary electrons responds relatively flatly to the kinetic energy of the incident ions and exhibits a broad maximum between 5 and 10 eV [75] (Fig. 2.32). The distributions for $E_i \leq 200$ eV are very similar; γ_i rises steeply for growing energies, and a maximum becomes visible at very low electron energies. Eventually, for the highest ion energies, the energy distribution of the secondaries peaks close to zero.
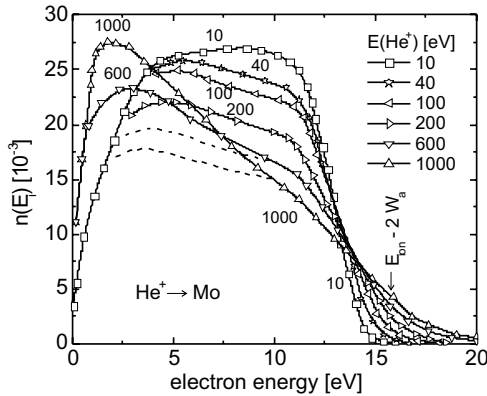
Fig. 2.32. Energy distribution of electrons which are released from a surface being atomically cleaned by He^+ ions with various kinetic energies. The dashed lines without symbols separate the AUGER processes from the other mechanisms which release secondary electrons [75] (© The American Physical Society).

An electron can be released only when the sum of the kinetic energy of the ion incident on the surface and the ionization potential exceeds twice the value of the work function W_a: For every electron emitted from the surface, a second one is required to neutralize the incident ion.

$$E_{\text{kin}}(e^-) \geq E_{\text{ion}} - 2\,W_a. \tag{2.60}$$

This condition is remarkably violated by neon which can be attributed to an additional AUGER process [76], and which is not observed when the electron is released by Ne ions of 10 eV kinetic energy. This strange phenomenon is explained by the discharging of ions of higher energy in close vicinity to the surface. Afterwards, these atoms can generate rapidly moving electrons in a process denoted AUGER relaxation. The yield of this process, however, exceeds that of the AUGER neutralization.

Typical values for the yield for secondary electrons, γ, vary between 0.05 and 0.1 for the heavy noble gases incident on molybdenum and tungsten (Fig. 2.33). The distinct energetic minimum of the number of secondary electrons for He^+ is absolutely striking. This is repeated for the heavier noble gas, however, to a weaker extent, which is due to a larger penetration depth with rising kinetic energy, and the electrons which are now released are attenuated during their course to the surface. This reduction in secondary electrons is overcompensated by the growth of the yield at further growing kinetic energies. For neon, this effect is covered by the above mentioned AUGER relaxation.[4] Although the curves of yield are very similar, the electron yield is

- always higher for molybdenum than for tungsten,

---

[4]This is valid for ion energies which are typical for glow discharges. Positive ions moving very rapidly (α-particles with energies of 1 MeV) can release up to thirty electrons; their energy amounts then to some keV.
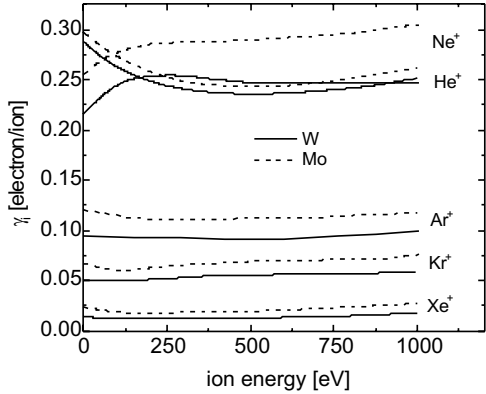
Fig. 2.33. Comparison of the yield for secondary electrons, γ_i, for the ions of the heavy noble gases incident on pure molybdenum and tungsten [75, 77] (© The American Physical Society).

- and depends on the ionization energy of the incident ion: The lower its ionization potential the less the yield of secondary electrons.

This is due to the low work function of molybdenum—for constant energy of the incident ions, the energy of the secondary electrons rises and enhances the probability of being released. On the other hand, FERMI energy and density of states at the FERMI level (this equals the number of conduction electrons divided by the FERMI energy in the free-electron model) energy and the number of released electrons: A falling FERMI energy causes a larger kinetic energy of the emitted electrons, simultaneously, the density of state goes up.

Furthermore, HAGSTRUM investigated the influence of the surface quality on the yield for secondary electrons [78]. Fig. 2.34 impressively illustrates the difficulties obtaining reliable data for δ and γ (γ as anisotropic property additionally depends on the crystal orientation).
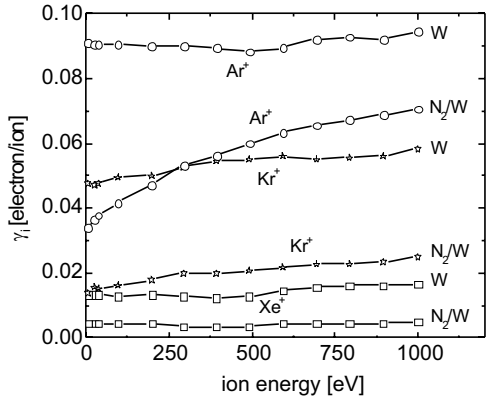

Fig. 2.34. γ_i as a function of kinetic energy of the heavy noble gas ions for pure tungsten and tungsten covered with a mono layer of nitrogen [78] (© The American Physical Society).

But also the energy distribution is altered by the contaminated surface: The fraction of rapid electrons is reduced. This is not only caused by a change in the work function but also by fundamental alterations of electron generation mechanisms with the exception of AUGER processes.

2.6.3 Photons

The electron yield caused by photons, triggered by the EINSTEINian photo effect, oscillates between 100 and 1000 ppm in the near UV (NUV) (dependent on the work function W_a) rising to values of up to 0.5 in the vacuum UV (VUV) (Figs. 2.35 and 2.36).
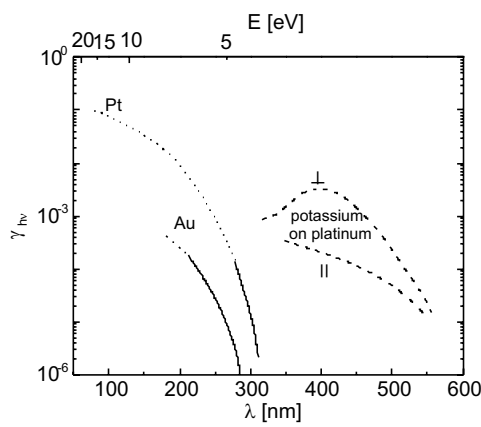

Fig. 2.35. Yield for photoelectrons $\gamma_{h\nu}$ of gold and platinum as functions of wavelength (lower abscissa) and energy (upper abscissa). $\gamma_{h\nu}$ additionally depends on the polarization of the incoming light [79]. $\perp$ and $\parallel$: $\boldsymbol{E}$ of linearly polarized light is orientated in perpendicular or in parallel fashion, respectively, with respect to the surface (© Oxford University Press).
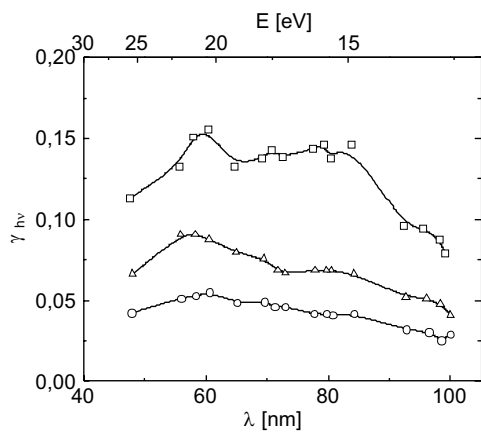

Fig. 2.36. The yield for photoelectrons depends sensitively on the pretreatment of the surface [80]: squares: untreated tungsten electrode; triangles: 5 min heated at $T > 1\,000$ °C and 10 Torr; circles: heated up to reproducibility at $T > 1\,000$ °C (© J. Wiley & Sons, Inc.).

Two main mechanisms have been identified which contribute to the steep increase in yield: First, most of the radiation in the long-wavelength range is reflected, and second, due to conservation of momentum, the excitation of free electrons in the valence band by a two-electron process seems very unlikely to happen. Going to short wavelengths, the reflectivities of the metals begin to decline to very low values (with simultaneous rise in transparency), and it becomes more likely to excite valence electrons.

All these observations add experimental proof to the suggestion that this process consists of two steps which both belong to the activation type with a certain threshold, generating the electrons as well as their escaping from the solid. Measuring the work function and the various coefficients γ, δ and η remains a great challenge still, since the yield depends strongly on the purity (volume property), but even more sensitively on the contamination (surface property). Theoretically, the main problem is the exact calculation of the barrier which has to be overcome (model potentials etc., cf. [81]).

Although the cross sections for photoionization are extremely small at low energies, this does not mean that they are without significance in glow discharges. In DC discharges, the charged carriers exhibit kinetic energies of several thousands of eV, therefore, photons of high energy are generated by AUGER processes.